



Geophysical Research Letters

RESEARCH LETTER

10.1029/2021GL094241

Key Points:

- · The ice core gas age-ice age difference (Δ age) is a powerful proxy for past surface temperature
- A simple analytical framework allows for reliable past temperature estimation using empirical estimates of Dage
- Low firn model sensitivity to accumulation rate contributes to published model-data mismatch of ice age firn thickness in East Antarctica

Correspondence to:

C. Buizert, Christo.buizert@oregonstate.edu

Citation:

Buizert, C. (2021). The ice core gas ageice age difference as a proxy for surface temperature. Geophysical Research Letters, 48, e2021GL094241. https://doi. org/10.1029/2021GL094241

Received 10 MAY 2021 Accepted 20 SEP 2021

The Ice Core Gas Age-Ice Age Difference as a Proxy for **Surface Temperature**

Christo Buizert¹



¹College of Earth, Ocean, and Atmospheric Sciences, Oregon State University, Corvallis, OR, USA

Abstract Ice cores provide detailed records of past climate change. Water stable isotopes are the most commonly used ice core climate proxy, but their quantitative interpretation remains challenging. Here, I argue that the gas age-ice age difference (Δ age) is a powerful proxy for past surface temperature. An analytical framework is derived that directly links past temperature to firn properties that can be reliably reconstructed (Δage, lock-in depth). The framework is calibrated using both present-day spatial patterns and last glacial maximum temperatures reconstructed via borehole thermometry. The usefulness of the method is demonstrated using three case studies from Greenland and Antarctic ice cores. The calibration suggests that several firn densification models, with the possible exception of the Herron-Langway model, have insufficient sensitivity to accumulation rates. This low sensitivity, in combination with large amplitude temperature forcing, can explain historical difficulties of densification models in simulating ice age firn thickness in East Antarctica.

Plain Language Summary It is important for scientists to understand past natural climate change. Ice cores drilled in the polar regions contain ancient ice up to 800,000 years old and can be used to reconstruct past climate. Ice from the polar regions contains air bubbles that are trapped at the bottom of the thick (50-120 m) perennial snow pack called the firn. The air in these bubbles is younger than the ice that surrounds it, and this age difference is called Δage. This paper develops a new method to estimate past temperatures of the ice sheet surface using our knowledge of changes in ice core Δage. The method is very simple and fast and agrees very well with independent temperature reconstructions where available.

"Since all models are wrong the scientist cannot obtain a 'correct' one by excessive elaboration. On the contrary following William of Occam (the scientist) should seek an economical description of natural phenomena." G. Box (1976)

1. Introduction and Background

1.1. Ice Core Climate Reconstruction

Temperature reconstructions from polar ice cores play an important role in paleoclimate research by virtue of their high temporal resolution and precise age control. Past temperatures allow estimation of climate sensitivity (Schmittner et al., 2011; Tierney et al., 2020), ice sheet response to past climate changes (Buizert et al., 2018; Clark et al., 2020; Simpson et al., 2009), and benchmarking climate models (Kageyama et al., 2021; Otto-Bliesner et al., 2021).

The stable isotope ratios of water (δ^{18} O and δ^{2} H) are widely used proxies for ice core site temperature (Dansgaard, 1964; Jouzel et al., 2003; Masson-Delmotte et al., 2008). The main challenge in interpretation is their calibration. Spatial and temporal regressions of $\delta^{18}O$ and site temperature yield very different values for the isotope sensitivity (Cuffey et al., 1995; Severinghaus et al., 1998). Isotope sensitivity is site-specific (Guillevic et al., 2013) and may vary through time (Kindler et al., 2014). While water isotopes provide unparalleled qualitative information, such as the timing and relative magnitude of climate change, additional sources of information are needed for quantitative interpretation.

Firn properties provide a means to obtain independent climate information from ice cores. Such information is encoded primarily in the gas age-ice age difference Δage (Schwander & Stauffer, 1984) and in δ^{15} N-N, via thermal and gravitational enrichment (Severinghaus et al., 1998; Sowers et al., 1992). Thermal

© 2021. American Geophysical Union. All Rights Reserved.

BUIZERT 1 of 12



fractionation in δ^{15} N provides accurate estimates of the magnitude of abrupt climate change in Greenland (Severinghaus et al., 1998), but not of long-term gradual changes such as the LGM-preindustrial temperature difference. Δ age provides a strong constraint on such gradual temperature changes, as first noted by Schwander et al. (1997) and more recently by Buizert et al. (2021; hereafter B21) and Kahle et al. (2021).

Previous efforts to extract climatic information from Δ age and $\delta^{15}N$ have all relied on dynamical firn densification modeling. Instead, the goal of this paper is to establish an analytical framework for linking past Δ age variations directly to surface temperature change.

1.2. Firn Dynamics and Δage Reconstruction

Firn is the transitional stage between surface snow and mature ice, in which the porous ice matrix gradually densifies under the overburden pressure of overlying strata (Cuffey & Paterson, 2010, Chapter 2). The firn is around 50–120 m thick, with high accumulation rate A and low surface temperature T contributing to a thicker firn. Interstitial pores remain connected with the overlying atmosphere, providing pathways for continued air movement and exchange. Vertical gas diffusion effectively halts at the lock-in depth L, at which point gravitational enrichment ceases and Δ age becomes fixed (Battle et al., 1996). Past variability in L is recorded directly in ice core δ^{15} N-N₂ via gravitational enrichment (Schwander, 1989; Sowers et al., 1992). The diffusive age of the air at L is usually negligible compared to the air of the ice at L (Buizert et al., 2013) and will here be ignored in calculations of Δ age.

The ice-equivalent lock-in depth $L_{\rm IE} = \int_0^L \! \rho(z) \, / \, \rho_{\rm ice} dz$, with ρ and $\rho_{\rm ice}$ the firn and ice densities respectively, reflects the amount of ice contained between the surface and L. The ratio $L_{\rm IE}/L$ has been found to be nearly constant across a wide range of climatic conditions, and is around 0.70 (Parrenin et al., 2012). Under (near-) steady-state accumulation, there is a fundamental relationship between Δ age and $L_{\rm IE}$:

$$\Delta age = \frac{L_{\rm IE}}{4}.\tag{1}$$

Historically, Δ age in Antarctica has been estimated using firn densification modeling. A newer development is to estimate it empirically via multi-core synchronization of the ice and gas phases via volcanic and methane (CH₄) stratigraphic matching, respectively (Baggenstos et al., 2018; Buizert et al., 2021; Epifanio et al., 2020; Menking et al., 2019). Empirical Δ age calculations are implicitly included also in multi-core frameworks such as IceChrono and the Antarctic ice core chronology (Parrenin et al., 2015; Veres et al., 2013). The WAIS Divide ice core is particularly useful in this regard, due to its small Δ age and high-resolution (cm-scale) CH₄ record (Rhodes et al., 2015), making it a "Rosetta stone" for understanding Δ age variability at other sites.

2. A Minimal Model Linking Δ age to Surface Temperature

2.1. Analytical Aage Framework

Traditional firn models subdivide the firn column into three stages with distinct rates of densification that reflect grain boundary sliding, grain sintering, and the compression of closed bubbles, respectively (Alley, 1987; Arnaud et al., 2000; Barnola et al., 1991; Herron & Langway, 1980). This work instead presents a single empirical relationship to capture the behavior of the firn column from the surface to the lock-in depth-corresponding roughly to the first two stages of densification.

The lock-in depth L scales as A divided by densification rate. Following Herron and Langway (1980), this gives the following scaling relationship

$$L \propto A^{\alpha} e^{E_T/RT}.$$
 (2)

With E_T the Arrhenius-type activation energy of firn densification, R the gas constant, and α a scaling factor $0 \le \alpha \le 1$ (Herron & Langway, 1980) that controls the sensitivity of densification rates to A. Using Equation 1, and the aforementioned observation that $L_{\rm IE}/L$ is constant across a wide range of climatic conditions, gives

$$\Delta age \propto A^{(\alpha-1)} e^{E_T/RT}, \tag{3}$$

BUIZERT 2 of 12



Equations 2 and 3 can be combined to define the accumulation-independent quantity:

$$\Delta \text{age} \cdot L^{\gamma} \propto e^{(1+\gamma)E_T/RT},$$
 (4)

with
$$\gamma = \frac{1 - \alpha}{\alpha}$$

Equation 4 can be used to directly link changes in observed firn properties (Δ age, L) to changes in site temperature, establishing a proxy relationship. Let T_1 and T_2 be the site temperature at two different climatic states, and Δ age, and Δ age, the corresponding Δ age, and L_1 and L_2 the corresponding L. Then,

$$\frac{\Delta age_1}{\Delta age_2} \cdot \left(\frac{L_1}{L_2}\right)^{\gamma} = e^{\frac{\left(1+\gamma\right)ET}{R}} \cdot \frac{\left(T_2-T_1\right)}{T_1T_2} \tag{5}$$

Treating $\overline{T}^2 = T_1 T_2$ as a constant, one can calculate the temperature difference:

$$T_2 - T_1 = \frac{R\overline{T}^2}{(1+\gamma)E_T} \ln \left[\frac{\Delta age_1}{\Delta age_2} \cdot \left(\frac{L_1}{L_2} \right)^{\gamma} \right].$$
 (6)

Equation 6 directly relates variations in Δ age, L and temperature, allowing firn properties to be used as an ice core temperature proxy. \overline{T} is the geometric mean temperature, but because $T_2 - T_1 \ll \overline{T}$, it can be approximated by the arithmetic mean temperature, or even T_1 or T_2 itself. Equation 6 is valid in Greenland and Antarctica and for all climatic states.

To calibrate the framework using present-day observations (Section 2.2.2), it is useful to introduce the common assumption that accumulation scales with local site temperature via the saturation vapor pressure (Fortuin & Oerlemans, 1990), as

$$A \propto e^{-E_A/RT}. (7)$$

Here, E_A is the apparent Arrhenius-type activation energy for the accumulation rate. This allows us to rewrite Equations 2 and 3 as:

$$L \propto e^{\left(E_T - \alpha E_A\right)/RT},\tag{8}$$

$$\Delta \text{age} \propto e^{\left(E_T + (1-\alpha)E_A\right)/RT} \ . \tag{9}$$

Last, the introduction of E_A allows us to use Δ age as a temperature proxy at sites where past L is unknown due to an absence of $\delta^{15}N$ data:

$$T_2 - T_1 = \frac{R\overline{T}^2}{E_\Delta} \ln \left[\frac{\Delta age_1}{\Delta age_2} \right], \tag{10}$$

with $E_{\Delta} = E_T + (1 - \alpha)E_A$. Because Equation 10 relies on E_A it should be interpreted with caution, as the T-A scaling is not constant in space and time (Fudge et al., 2016; Lee et al., 2020; Monnin et al., 2004). Whenever δ^{15} N data are available, Equation 6 should therefore be used instead.

2.2. Calibration of the Analytical Δ age Framework

2.2.1. Firn Densification Model Comparison

Here, I evaluate the mathematical framework by comparing it to established firn densification models. Figure 1 shows L and Δ age as a function of T and A for four different firn models commonly used in ice core research (solid lines): the Herron-Langway (HL) model (Herron & Langway, 1980), the Barnola model (Barnola et al., 1991; Schwander et al., 1997), the Arnaud model (Arnaud et al., 2000; Goujon et al., 2003), and the Bréant model (Bréant et al., 2017). I then find the α and E_T values that optimize the fit of the new framework to the densification models (see caption for details). The HL, Barnola, and Arnaud models can be well approximated with the framework, yet the Bréant model cannot due to the strongly curved isopleths that arise from the hypothesized existence of multiple activation energies in that model.

The α reflects the effective sensitivity of the model to A. For $\alpha=0$, L becomes independent of A (vertical L-isopleths in Figure 1). The Arnaud and Barnola models have low sensitivity to A ($\alpha=0.24$), and the HL model has a higher sensitivity ($\alpha=0.39$). The effective E_T values are 15.5, 16.0, and 20.0 kJ mol⁻¹ for the

BUIZERT 3 of 12

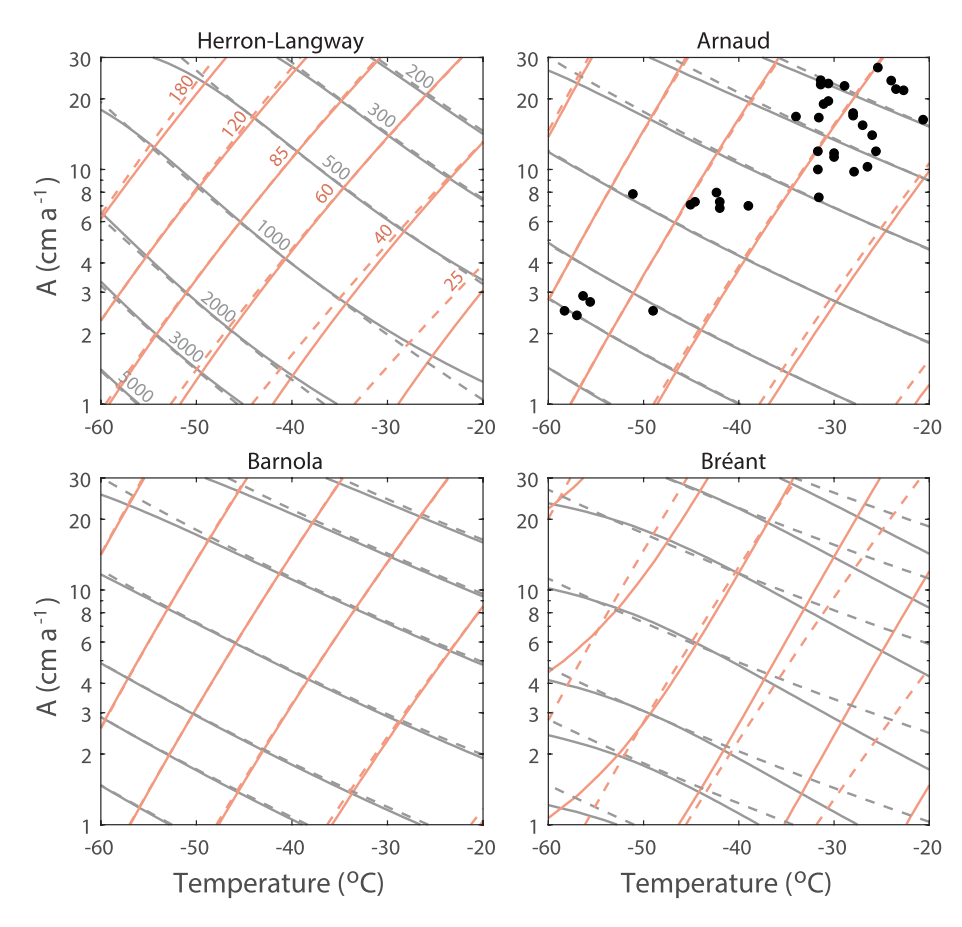


Figure 1. Comparison to firn densification models. Isopleths of Δ age (gray) and L (salmon) as a function of T and A at the site for a steady-state climate. The solid lines show the various densification models as specified at the top of each panel; the dashed lines provide the best fit using the simplified mathematical framework. The same Δ age and L values are contoured in all panels, with numeric values given in upper left panel. Upper right panel shows modern-day climatic conditions at a wide range of well-characterized sites in Greenland and Antarctica (black dots). The α and E_T values selected minimize the RMS offset between the firn model L and Equation 2; a constant scaling is applied such that Equation 2 gives an L identical to the firn model at $T = -40^{\circ}\text{C}$ and $A = 8 \text{ cm a}^{-1}$.

Barnola, Arnaud, and HL models, respectively. These effective $E_{\rm T}$ values give the temperature sensitivity when densification is defined in terms of accumulation rates; models tend to have a higher activation energy when defined in terms of overburden pressure (60.0, 60.0, and 42.8 kJ mol⁻¹ for stage 2 in the Barnola, Arnaud, and HL models, respectively).

2.2.2. Modern-Day Spatial Patterns

Fitting Δ age and L shows that the former scales more strongly with temperature. From Equation 1, the relationship $E_{\Delta} = E_A + E_L$ is expected, which is satisfied within uncertainty. Following Equations 8 and 9, let $E_{\Delta} = E_T + (1 - \alpha)E_A$ and $E_L = E_T - \alpha E_A$; inserting the fitted values and averaging the two equations gives $E_T = E_A \alpha + 10.4 = 26.1\alpha + 10.4$ kJ mol⁻¹. Clearly the problem is under-constrained: rather than a single

BUIZERT 4 of 12

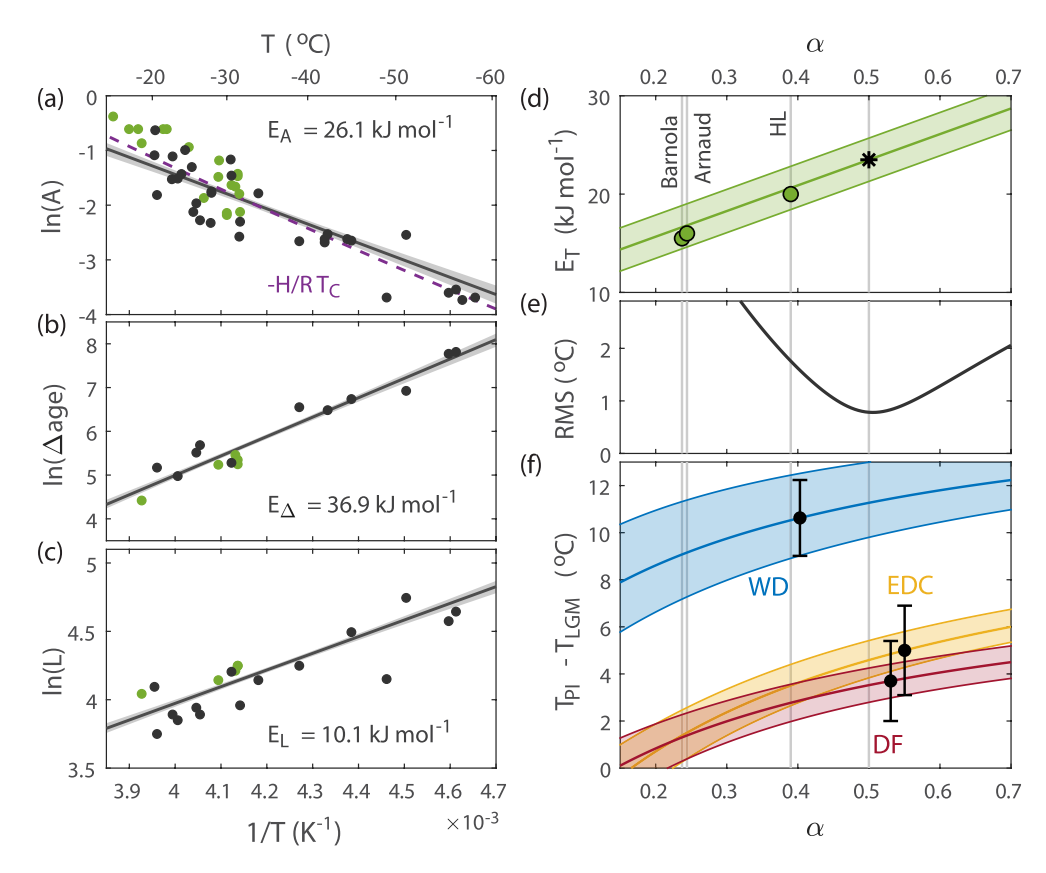


Figure 2. Calibration of Δage framework. (a)–(c) Arrhenius plots for A, Δage and L with apparent activation energy derived from linear regression (gray line with uncertainty envelope). Sites are from Antarctica (black) and Greenland (green); all regressions are applied only to those sites for which all parameters (T, T, T, and Δage) are known. In a 10,000 iteration Monte Carlo study all site data are perturbed randomly within their uncertainty prior to regression analysis; this suggests T0 uncertainties of 2.5, 2.2, and 0.7 kJ mol⁻¹ for T1 for T2, and T3 and T4 the purple dashed line gives the slope T4 slope T5 with T6 the enthalpy of sublimation (51 kJ mol⁻¹) and T5 the condensation temperature following T6 and T7 the condensation temperature following T8 slope T9 (Jouzel & Merlivat, 1984). (d) Firn thermal activation energy T8 as function of T9 with uncertainty (green line with shaded area), results from firn model fitting (green dots) and recommended values (asterisk). (e) and (f) Calibration using LGM temperatures from borehole thermometry for WD (blue), EDC (yellow) and DF (red). For EDC, the average of two ice flow thinning scenarios (one with, and one without ice divide migration) is used (see B21). The model-data RMS misfit is minimized for T9 conditions are from the properties of the second structure of the properties of the second structure of the properties of T9 conditions are from the properties of T9 conditions and T9 conditions are from the properties of T9 conditions are fro

optimal value of α and E_T , the solutions fall on a line. The $\left\{\alpha, E_T\right\}$ fitting parameters from the firn densification models (Section 2.2.1) agree with the spatially calibrated framework within uncertainty (Figure 2d). This calibration exercise highlights a fundamental problem in firn densification modeling, namely that the model sensitivities to A and T are non-uniquely constrained by modern firn data alone due to the strong covariation of A and T in the climate system. The HL, Arnaud, and Barnola models fit firn density data equally well, yet they do so with very different effective sensitivities to A and T.

2.2.3. Borehole Thermometry

In modern observations, L increases in a colder climate (Figure 2c), yet during the colder LGM, L actually decreases at several East Antarctic sites; this suggests a climate shift that does not follow the modern spatial T-A scaling. The LGM thus provides a unique opportunity for firn model calibration outside of the modern spatial pattern.

Borehole thermometry provides independent constraints on LGM surface temperature (Cuffey et al., 1995, 2016; Dahl-Jensen et al., 1998; Johnsen et al., 1995). Here, the focus is on Antarctica, using borehole thermometry estimates from Cuffey et al. (2016) for the WAIS Divide (WD) core and B21 for the EPICA Dome C (EDC) and Dome Fuji (DF) sites. In these studies, the temperature-water isotope scaling is calibrated by optimizing the fit to the observed borehole temperature profile; the methodology from Cuffey

BUIZERT 5 of 12



et al. (2016) differs slightly from B21 in that it also incorporates information about past L (from $\delta^{15}N$ data) to improve the borehole temperature fit.

Combining Equation 6 with the spatial calibration result ($E_T = 26.1\alpha + 10.4 \, \mathrm{kJ \ mol^{-1}}$), the LGM-preindustrial surface temperature change is calculated at WD, EDC, and DF as a function of α and compared to the results from borehole thermometry (Figure 2f). Preindustrial and LGM estimates of Δ age and L are taken from B21. The root-mean-square (RMS) offset between the borehole thermometry results and Equation 6 is minimized for $\alpha = 0.50$ (Figure 2e). Based on combined results from the spatial and LGM calibration studies, I recommend using values of $\alpha = 0.50 \pm 0.05$ and $E_T = 23.5 \pm 2.2 \, \mathrm{kJ \ mol^{-1}}$ in Equation 6 for paleoclimate applications (Figure 2d, asterisk).

2.2.4. Using the Framework Without $\delta^{15}N$ Data

For ice cores or depth ranges where $\delta^{15}N$ data are not available yet empirical Δ age estimates are, Equation 10 can be used to estimate past T. The value of the denominator E_{Δ} that minimizes the 7-site RMS offset between Equation 6 and 10 is $E_{\Delta} = 46.6$ kJ mol $^{-1}$ (Figure 3a); note that, this is similar to Equation 6 denominator $(1+\gamma)E_T = 47$ kJ mol $^{-1}$ because the L ratio is close to unity (range of 0.87–1.1 for the sevenn Antarctic sites). While Equation 6 works in both Greenland and Antarctica, the presented calibration of Equation 10 only works in Antarctica as it relies on the temporal T-A relationship that may be different for the two ice sheets. Because the T-A scaling varies through time (Fudge et al., 2016), a conservative uncertainty for E_{Δ} of 10 kJ mol $^{-1}$ is recommended.

2.3. Recommendations for Use of the Δ age Framework

I recommend users follow these steps in applying the framework:

- 1. Estimate Δ age empirically. This can be done in multiple ways: (a) Multi-core synchronization of both ice-phase (ideally volcanic) and gas-phase (ideally CH $_4$) to a core that has a small and relatively well known Δ age. (b) Matching ice-phase and gas-phase markers in a single core. For example, the δ^{15} N-N $_2$ and δ^{18} O-ice during Greenland Dansgaard-Oeschger events. (c) The Δ depth method developed by Parrenin et al. (2012) that is built into the IceChrono software (Parrenin et al., 2015). (d) Present-day Δ age can be estimated from firn air sampling data (ice age at the lock-in depth).
- 2. If available, estimate the diffusive column thickness D from $\delta^{15}N$ data using $\delta^{15}N = 10^3 \Delta MgD/RT$ with ΔM being the mass difference (1 × 10⁻³ kg mol⁻¹) and g being the gravitational acceleration. To find L, add a convective zone thickness to D; typically this zone is between 0 and 6 m thick (Kawamura et al., 2006). At low-accumulation sites, a geothermal correction may be applied: one can estimate the temperature difference between surface and L using Equation 9.17 from Cuffey and Paterson (2010), and add 3 m to L for every degree of geothermal temperature difference between the surface and lock-in depth.
- 3. Establish the reference time. Using the modern-day site, conditions is recommended, because Δ age and L can be estimated most accurately. This reference period has temperature T_1 in Equation 6.
- 4. Apply Equation 6 with $\alpha=0.50\pm0.05$ and $E_{\rm T}=23.5\pm2.2$ kJ mol $^{-1}$ if L data are available. If L data are unavailable, use Equation 10 with $E_{\Delta}=46.6\pm10$ kJ mol $^{-1}$ (Antarctica only).
- 5. The state of the firn is determined by the average climate over a previous number of years roughly equal to Δ age. Assign the interval midpoint age to the temperature estimate: use the ice age at the depth of the gas feature used to empirically estimate Δ age, and subtract Δ age/2 (equivalently, use the gas age and add Δ age/2)
- 6. In Greenland ice cores, consider whether your data point is close to steady-state (e.g., at the end of a stable climatic period). If not, discard.
- 7. Propagate the uncertainty in L, Δ age, α , and $E_{\rm T}$ to get the uncertainty of the calculated temperature anomaly.

BUIZERT 6 of 12

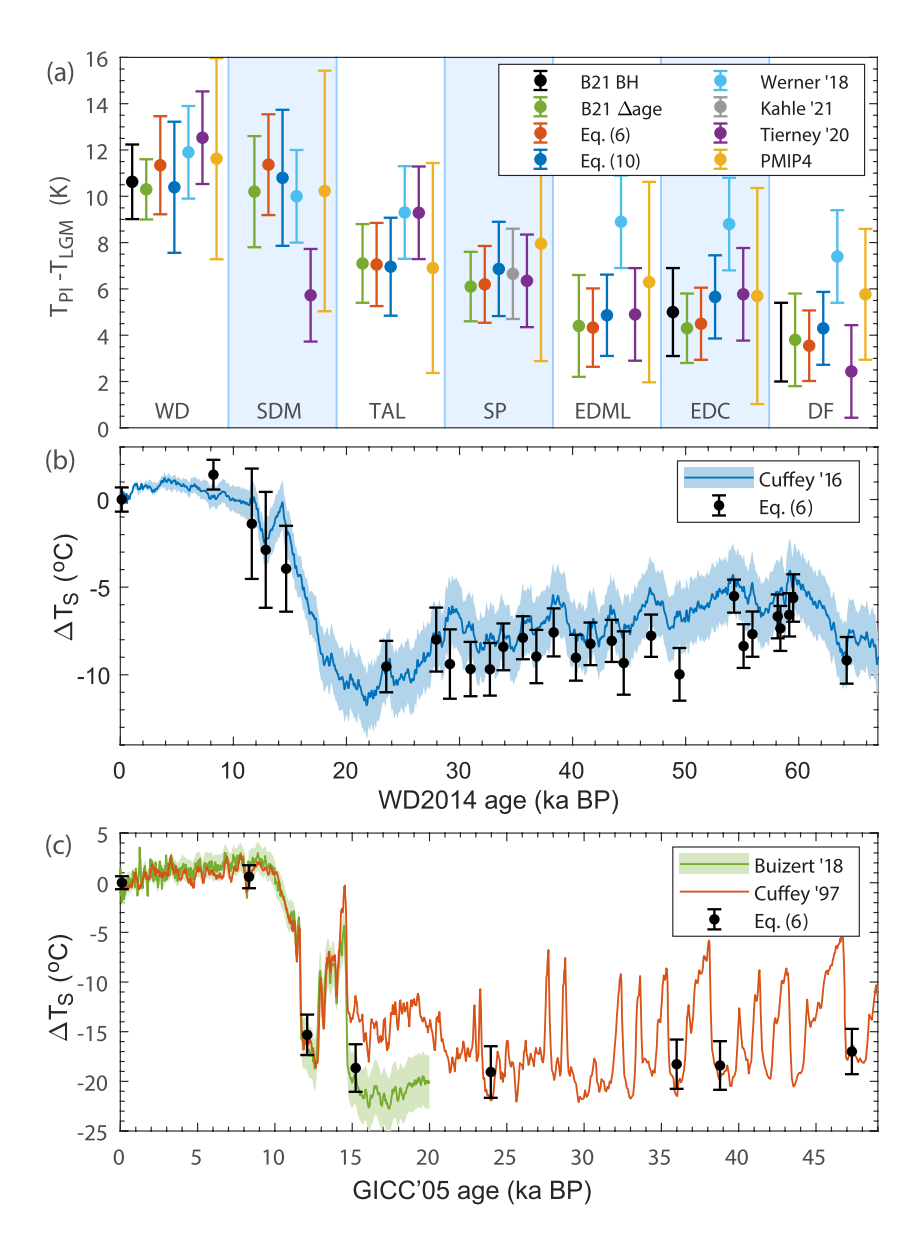


Figure 3. Δage-based temperature reconstruction: three case studies. (a) Seven-site comparison of the results by Buizert et al. (2021), Kahle et al. (2021), Tierney et al. (2020), Werner et al. (2018), and PMIP4 (Kageyama et al., 2021); a 2°C uncertainty is assigned to the Werner and Tierney reconstructions. WD, WAIS Divide; SDM, Siple Dome; TAL, Talos Dome; SP, South Pole; EDML, EPICA (European Project for Ice Coring in Antarctica) Dronning Maud Land; EDC, EPICA Dome C; DF, Dome Fuji. (b) Borehole-based reconstruction for WAIS Divide in blue with uncertainty envelope (Cuffey et al., 2016), Δage-based WD estimates using Equation 6 as black dots with error bars. (c) Borehole-based GISP2 reconstruction in orange (Cuffey & Clow, 1997), firn-densification based GISP2 reconstruction in green with uncertainty envelope (Buizert et al., 2018), Δage-based GISP2 estimates using Equation 6 as black dots with error bars. Equation 6 uncertainties are founded by adding in quadrature the uncertainties related to α, E_T , Δage, and E_T

3. Discussion

3.1. Three Case Studies

3.1.1. Case 1: Antarctic-Wide Last Glacial Maximum Temperatures

First, I revisit the LGM temperature reconstruction from B21 (Figure 3a). The current method with Equation 6 provides a good fit to the borehole estimates at WD, EDC and DF, which is by construction given that the borehole estimates were used in the calibration. The current method also provides a good fit to the B21 firn-densification modeling at the other four sites. The Δ age and L estimates used here are identical to those

BUIZERT 7 of 12



used in B21; this comparison demonstrates that the current simplified Δ age framework provides nearly identical results to a full firn modeling study, yet with significantly less work involved.

The spatial pattern of LGM cooling in Antarctica is attributed to the pattern of LGM-preindustrial elevation changes (Buizert et al., 2021; Werner et al., 2018). For comparison, Figure 3a further shows independent LGM surface cooling estimates based on water isotope diffusion lengths in the South Pole ice core (Kahle et al., 2021), paleo data-assimilation (Tierney et al., 2020), PMIP4 climate model simulations (Paleoclimate Model Intercomparison Project Phase 4; Kageyama et al., 2021), and traditional interpretation of water isotopes calibrated via the spatially calibrated slope (Werner et al., 2018). The smaller magnitude of LGM cooling in East Antarctica as found by B21 agrees well with the independent estimates from PMIP4 and Tierney et al. (2020). Note, however, that the latter two studies find less low-latitude LGM cooling than was recently reconstructed using groundwater noble gas ratios (Seltzer et al., 2021).

3.1.2. Case 2: WAIS Divide Temperature History

Second, I apply Equation 6 to the Antarctic WAIS Divide ice core (Figure 3b). With a large ice thickness (3,450 m) and high accumulation rate (22 cm $\rm a^{-1}$ ice equivalent), WD has the optimal characteristics for borehole thermometry (Cuffey et al., 2016). Empirical WD Δ age constraints from B21 are found by combining volcanic and CH₄ stratigraphic matching to Greenland ice cores (Svensson et al., 2020; Veres et al., 2013); estimates of L are derived from the WD δ ¹⁵N record (Buizert et al., 2015).

The Δ age and borehole reconstruction methods agree within uncertainty at all depths considered (Figure 3b); this is not an independent validation of the Δ age method because the WD borehole reconstruction was used as part of the calibration. The Δ age method confirms much of the millennial-scale climate change of the glacial period derived from δ^{18} O of ice. Surprisingly, the Δ age method finds no Antarctic cold reversal (ACR, 14.7–12.8 ka BP), however an ACR cannot be ruled out due to the larger uncertainty at this time, and the violation of the steady-state assumption. The Δ age method systematically finds around 1.5°C lower temperatures during marine isotope stage 3 (MIS 3, 27–60 ka BP). This mismatch is consistent with the fact that the empirical WD Δ age values from B21 during this period are about 70 years greater than earlier calculations using the borehole-based WD temperature reconstruction (Buizert et al., 2015). The Δ age method further suggests a slightly different structure for the WD Holocene temperature trend, with higher temperatures around 8 ka, and lower temperatures at the Holocene onset and deglaciation.

3.1.3. Case 3: GISP2 Temperature History

Third, I apply Equation 6 to the Greenland GISP2 ice core (Figure 3c), where the first reliable borehole temperature reconstructions were made (Cuffey & Clow, 1997; Cuffey et al., 1995). Data-based Δ age constraints are derived from the (layer-counted) age difference between the $\delta^{15}N$ (gas phase) and $\delta^{18}O$ (ice phase) signals associated with abrupt climate change; estimates of L are derived from the GISP2 $\delta^{15}N$ data (Seierstad et al., 2014). Empirical Δ age estimates at the onset of abrupt climate change events are used, at which point the firn column should be close to steady state.

The Δ age method provides good agreement with independent prior reconstructions from borehole thermometry (Cuffey & Clow, 1997) and detailed dynamical firn modeling (Buizert et al., 2014, 2018). The Δ age method finds a Younger Dryas (12.8–11.6 ka BP) temperature that matches both other methods. During MIS 3, the Δ age method agrees with the borehole-based reconstruction. At the onset of the Bølling-Allerød (14.7 ka BP), the method disagrees with the borehole calibration, yet it agrees with the firn-based reconstruction. This is not surprising given that both firn-based reconstructions rely on the same $\delta^{15}N$ data. Note that the method presented here is at least an order of magnitude less work than a full dynamical firn densification study.

3.2. Lessons on Firn Densification Physics

The new method provides a consistent way to compare and quantify densification model steady-state behavior (Figures 1 and 2d). The Barnola and Arnaud models have lower accumulation sensitivity than the HL model (smaller α , steeper L-isopleths). Of these three, the HL model is closest to the calibration of α based on independent observations from LGM borehole thermometry. Therefore, I here suggest that the Herron-Langway model has the most accurate response to climate variability, and therefore should be

BUIZERT 8 of 12



the preferred model in modeling of past firn properties. Indeed, the Barnola and Arnaud models produce LGM-preindustrial temperature changes much smaller than those reconstructed from borehole thermometry at EDC and DF (Figure 2e and B21, Figure S9). To better constrain α , detailed studies are needed at sites that deviate strongly from the average T-A scaling (Figure 2a), that is, high T-low A or low T-high A. Taylor Dome, Antarctica, would be a promising candidate site for such a study because it has a large spatial gradient in A at a fairly constant T (Morse et al., 1999).

The Bréant model is a modified version of the Arnaud model with a complex temperature response due to the use of three activation energies (1.5, 75, and 110 kJ mol^{-1}). The simple Δ age framework cannot capture its response adequately (Figure 1). B21 shows that the Bréant model gives comparable LGM temperature solutions to the HL model at the WD, DF and EDC sites, in agreement with borehole thermometry. It thus appears to be a valid alternative to the HL model. However, at low T, the Bréant model relies on activation energies much lower than those of known physical firn process. This low value is not needed to fit modern observations, but rather an attempt to fit LGM δ^{15} N data at East Antarctic sites (e.g., EDC) when forcing the model with a large (\sim 9°C) LGM-preindustrial temperature change.

A correlation exists between Calcium concentration and firn density on the cm-scale, yet there is no mechanistic understanding of this link (Freitag et al., 2013; Hörhold et al., 2012). Including the hypothesized dust softening effect in simulations of glacial-interglacial firn dynamics does not systematically improve the fit to observations (such as δ^{15} N); in many cases, it worsens the fit (Bréant et al., 2017; Buizert et al., 2015, 2021). In the cores investigated here, Ca concentrations range from ~0.8 ppb in the Holocene at WD (Markle et al., 2018) to over 400 ppb in stadials at GISP2 (Mayewski et al., 1997). Yet, a simple scaling law with two tunable parameters (α , $E_{\rm T}$) appears capable of capturing the T- Δ age relationship in these cores within the uncertainty of the reconstructions (Figures 3b and 3c); this supports the idea that Ca concentrations have at most a minor influence on glacial-interglacial firn dynamics.

3.3. The $\delta^{15}N$ Model-Data Mismatch in Antarctic Glacial Climates

Previous firn densification studies have reported difficulty in fitting the relatively small glacial firn column thickness indicated by $\delta^{15}N$ in East Antarctic sites (Bréant et al., 2017; Capron et al., 2013; Landais et al., 2006). Here, I follow recent studies that suggest that using realistic forcings for LGM T and A, densification models can successfully fit LGM $\delta^{15}N$ in East Antarctica (Buizert et al., 2021; Kahle et al., 2021). This section briefly explores the $\delta^{15}N$ model-data mismatch.

The original paper on this topic suggests that uncertainty in the model forcing, particularly accumulation, is a likely origin of the mismatch (Landais et al., 2006). With advances in empirical Δ age estimation and L derived from $\delta^{15}N$ data, one can obtain accurate A estimates via Equation 1. Because Equation 1 is built into the Δ age framework, all solutions found via Equation 6 are automatically consistent with past A. Theoretical firn models with accumulation sensitivities $0 \le \alpha \le 1$ are tested (Figure 2e), and none of these obtain a LGM-preindustrial temperature difference of 9°C at EDC as found via the spatial-slope calibration method (Masson-Delmotte et al., 2010). Thus, the $\delta^{15}N$ model-data mismatch cannot be solved via uncertainty in A as long as a 9°C T forcing is applied. Using T forcing at DF and EDC consistent with borehole-thermometry estimates can provide a consistent solution over a range of α (Figures 2e and 2f). This is the main solution to the $\delta^{15}N$ mismatch problem, in the view of the author.

Model physics also plays a role. The calibration study finds that the Arnaud and Barnola models have low sensitivity to A (small α , see Figure 2d), which results in high LGM $\delta^{15}N$ even when forced with relatively small LGM cooling. This observation agrees with Capron et al. (2013) who, using the Arnaud/Goujon model, suggest that the model is insufficiently sensitive to A. The extensive use of the Arnaud/Goujon model in the literature has thus likely contributed to the perception of a glacial model-data mismatch in $\delta^{15}N$.

BUIZERT 9 of 12



Acknowledgments

and 2102944).

The author thank two anonymous

substantially improved this study.

reviewers whose thoughtful comments

The author further thank anonymous

reviewer #3 from B21 whose review,

though strongly favoring rejection of

that paper, provided the impetus to per-

author gratefully acknowledge financial

form the analyses described here. The

support from the US National Science

Foundation (awards 1643394, 1702920,

4. Concluding Remarks

The ice core gas age-ice age difference, or Δ age, is a powerful proxy for past surface temperature. The analytical framework presented here allows past temperature to be calculated directly from reconstructed firn properties (Δ age and L). A calibration study further suggests that in particular the Arnaud and Barnola models underestimate the sensitivity of firn densification to accumulation rates.

This work emphasizes the need for understanding the physical environment of snow deposition in ice cores. High resolution CH_4 and $\delta^{15}N-N_2$ records along the full ice core depth should be a high priority for all ice core projects, as well as firn air sampling to document present-day firn characteristics.

Conflict of Interest

The authors declare no conflicts of interest relevant to this study.

Data Availability Statement

The reconstructions from this study are available in the data supplement and at https://www.ncdc.noaa.gov/paleo-search/study/34133. This study uses previously published data sets that are publicly available via online databases (https://doi.org/10.15784/600377, https://www.ncdc.noaa.gov/paleo-search/study/2475 and https://www.ncdc.noaa.gov/paleo/study/32632).

References

- Alley, R. B. (1987). Firn densification by grain-boundary sliding—A 1st model. *Journal de Physique*, 48(C-1), 249–256. https://doi.org/10.1051/jphyscol:1987135
- Arnaud, L., Barnola, J. M., & Duval, P. (2000). Physical modeling of the densification of snow/firn and ice in the upper part of polar ice sheets. In T. Hondoh (Ed.), *Physics of ice core records* (pp. 285–305).
- Baggenstos, D., Severinghaus Jeffrey, P., Mulvaney, R., McConnell Joseph, R., Sigl, M., Maselli, O., et al. (2018). A horizontal ice core from Taylor Glacier, its implications for Antarctic climate history, and an improved Taylor Dome Ice Core Time Scale. *Paleoceanography and Paleoclimatology*, 33, 778–794. https://doi.org/10.1029/2017pa003297
- Barnola, J. M., Pimienta, P., Raynaud, D., & Korotkevich, Y. S. (1991). CO2-climate relationship as deduced from the Vostok ice core: A re-examination based on new measurements and on a re-evaluation of the air dating. *Tellus Series B Chemical and Physical Meteorology*, 43(2), 83–90. https://doi.org/10.3402/tellusb.y43i2.15249
- Battle, M., Bender, M., Sowers, T., Tans, P. P., Butler, J. H., Elkins, J. W., et al. (1996). Atmospheric gas concentrations over the past century measured in air from firn at the South Pole. *Nature*. 383(6597), 231–235. https://doi.org/10.1038/383231a0
- Box, G. E. P. (1976). Science and statistics. *Journal of the American Statistical Association*, 71(356), 791–799. https://doi.org/10.1080/0162 1459.1976.10480949
- Bréant, C., Martinerie, P., Orsi, A., Arnaud, L., & Landais, A. (2017). Modelling firn thickness evolution during the last deglaciation: Constraints on sensitivity to temperature and impurities. *Climate of the Past*, 13(7), 833–853. https://doi.org/10.5194/cp-13-833-2017
- Buizert, C., Cuffey, K. M., Severinghaus, J. P., Baggenstos, D., Fudge, T. J., Steig, E. J., et al. (2015). The WAIS divide deep ice core WD2014 chronology—Part 1: Methane synchronization (68–31 ka BP) and the gas age-ice age difference. Climate of the Past, 11, 153–173. https://doi.org/10.5194/cp-11-153-2015
- Buizert, C., Fudge, T. J., Roberts, W. H. G., Steig Eric, J., Sherriff-Tadano, S., Ritz, C., et al. (2021). Antarctic surface temperature and elevation during the last glacial maximum. Science, 372(6546), 1097–1101. https://doi.org/10.1126/science.abd2897
- Buizert, C., Gkinis, V., Severinghaus, J. P., He, F., Lecavalier, B. S., Kindler, P., et al. (2014). Greenland temperature response to climate forcing during the last deglaciation. *Science*, 345(6201), 1177–1180. https://doi.org/10.1126/science.1254961
- Buizert, C., Keisling, B. A., Box, J. E., He, F., Carlson, A. E., Sinclair, G., & DeConto, R. M. (2018). Greenland-wide seasonal temperatures during the last deglaciation. *Geophysical Research Letters*, 45(4), 1905–1914. https://doi.org/10.1002/2017gl075601
- Buizert, C., Sowers, T., & Blunier, T. (2013). Assessment of diffusive isotopic fractionation in polar firn, and application to ice core trace gas records. Earth and Planetary Science Letters, 361(0), 110–119. https://doi.org/10.1016/j.epsl.2012.11.039
- Capron, E., Landais, A., Buiron, D., Cauquoin, A., Chappellaz, J., Debret, M., et al. (2013). Glacial-interglacial dynamics of Antarctic firn columns: Comparison between simulations and ice core air-δ¹⁵N measurements. *Climate of the Past*, *9*(3), 983–999. https://doi.org/10.5194/cp-9-983-2013
- Clark, P. U., He, F., Golledge, N. R., Mitrovica, J. X., Dutton, A., Hoffman, J. S., & Dendy, S. (2020). Oceanic forcing of penultimate deglacial and last interglacial sea-level rise. *Nature*, 577(7792), 660–664. https://doi.org/10.1038/s41586-020-1931-7
- Connolley, W. (1996). The Antarctic temperature inversion. International Journal of Climatology: A Journal of the Royal Meteorological Society, 16(12), 1333–1342. https://doi.org/10.1002/(sici)1097-0088(199612)16:12<1333::aid-joc96>3.0.co;2-6
- Cuffey, K. M., & Clow, G. D. (1997). Temperature, accumulation, and ice sheet elevation in central Greenland through the last deglacial transition. *Journal of Geophysical Research*, 102(C12), 26383–26396. https://doi.org/10.1029/96jc03981
- Cuffey, K. M., Clow, G. D., Alley, R. B., Stuiver, M., Waddington, E. D., & Saltus, R. W. (1995). Large Arctic temperature change at the Wisconsin-Holocene glacial transition. *Science*, 270(5235), 455–458. https://doi.org/10.1126/science.270.5235.455
- Cuffey, K. M., Clow, G. D., Steig, E. J., Buizert, C., Fudge, T. J., Koutnik, M., et al. (2016). Deglacial temperature history of West Antarctica. Proceedings of the National Academy of Sciences, 113, 14249–14254. https://doi.org/10.1073/pnas.1609132113
 Cuffey, K. M., & Paterson, W. S. B. (2010). The physics of glaciers (4th ed.). Butterworth-Heinemann.

BUIZERT 10 of 12



- Dahl-Jensen, D., Mosegaard, K., Gundestrup, N., Clow, G. D., Johnsen, S. J., Hansen, A. W., & Balling, N. (1998). Past temperatures directly from the Greenland Ice Sheet. *Science*, 282(5387), 268–271. https://doi.org/10.1126/science.282.5387.268
- Dansgaard, W. (1964). Stable isotopes in precipitation. Tellus, 16(4), 436-468. https://doi.org/10.3402/tellusa.v16i4.8993
- Epifanio, J. A., Brook, E. J., Buizert, C., Edwards, J. S., Sowers, T. A., Kahle, E. C., et al. (2020). The SP19 chronology for the South Pole Ice Core—Part 2: Gas chronology, delta age, and smoothing of atmospheric records. *Climate of the Past*, 2020(16), 2431–2444. https://doi.org/10.5194/cp-16-2431-2020
- Fortuin, J., & Oerlemans, J. (1990). Parameterization of the annual surface temperature and mass balance of Antarctica. *Annals of Glaciology*, 14, 78–84. https://doi.org/10.3189/s0260305500008302
- Freitag, J., Kipfstuhl, J., Laepple, T., & Wilhelms, F. (2013). Impurity-controlled densification: A new model for stratified polar firn. *Journal of Glaciology*, 59(218), 1163–1169. https://doi.org/10.3189/2013jog13j042
- Fudge, T. J., Markle, B. R., Cuffey, K. M., Buizert, C., Taylor, K. C., Steig, E. J., et al. (2016). Variable relationship between accumulation and temperature in West Antarctica for the past 31,000 years. *Geophysical Research Letters*, 43(8), 2016GL068356. https://doi.org/10.1002/2016gl068356
- Goujon, C., Barnola, J. M., & Ritz, C. (2003). Modeling the densification of polar firn including heat diffusion: Application to close-off characteristics and gas isotopic fractionation for Antarctica and Greenland sites. *Journal of Geophysical Research*, 108(D24), 18. https://doi.org/10.1029/2002jd003319
- Guillevic, M., Bazin, L., Landais, A., Kindler, P., Orsi, A., Masson-Delmotte, V., et al. (2013). Spatial gradients of temperature, accumulation and delta18O-ice in Greenland over a series of Dansgaard-Oeschger events. *Climate of the Past*, 9(3), 1029–1051. https://doi.org/10.5194/cp-9-1029-2013
- Herron, M. M., & Langway, C. C. (1980). Firn densification: An empirical model. *Journal of Glaciology*, 25(93), 373–385. https://doi.org/10.3189/s0022143000015239
- Hörhold, M. W., Laepple, T., Freitag, J., Bigler, M., Fischer, H., & Kipfstuhl, S. (2012). On the impact of impurities on the densification of polar firn. Earth and Planetary Science Letters, 325–326, 93–99. https://doi.org/10.1016/j.epsl.2011.12.022
- Johnsen, S. J., Dahl-Jensen, D., Dansgaard, W., & Gundestrup, N. (1995). Greenland palaeotemperatures derived from GRIP bore hole temperature and ice core isotope profiles. *Tellus B: Chemical and Physical Meteorology*, 47, 624–629. https://doi.org/10.1034/j.1600-0889.47. issue5.9.x
- Jouzel, J., & Merlivat, L. (1984). Deuterium and oxygen 18 in precipitation: Modeling of the isotopic effects during snow formation. *Journal of Geophysical Research*, 89(D7), 11749–11757. https://doi.org/10.1029/jd089id07p11749
- Jouzel, J., Vimeux, F., Caillon, N., Delaygue, G., Hoffmann, G., Masson-Delmotte, V., & Parrenin, F. (2003). Magnitude of isotope/ temperature scaling for interpretation of central Antarctic ice cores. *Journal of Geophysical Research*, 108(D12), 4361. https://doi. org/10.1029/2002id002677
- Kageyama, M., Harrison, S. P., Kapsch, M. L., Lofverstrom, M., Lora, J. M., Mikolajewicz, U., et al. (2021). The PMIP4 last glacial maximum experiments: Preliminary results and comparison with the PMIP3 simulations. Climate of the Past, 17(3), 1065–1089. https://doi.org/10.5194/cp-17-1065-2021
- Kahle, E. C., Steig, E. J., Jones, T. R., Fudge, T. J., Koutnik, M. R., Morris, V. A., et al. (2021). Reconstruction of temperature, accumulation rate, and layer thinning from an ice core at South Pole, using a statistical inverse method. *Journal of Geophysical Research: Atmospheres*, 126(13), e2020JD033300. https://doi.org/10.1029/2020jd033300
- Kawamura, K., Severinghaus, J. P., Ishidoya, S., Sugawara, S., Hashida, G., Motoyama, H., et al. (2006). Convective mixing of air in firn at four polar sites. *Earth and Planetary Science Letters*, 244(3–4), 672–682. https://doi.org/10.1016/j.epsl.2006.02.017
- Kindler, P., Guillevic, M., Baumgartner, M., Schwander, J., Landais, A., & Leuenberger, M. (2014). Temperature reconstruction from 10 to 120 kyr b2k from the NGRIP ice core. Climate of the Past, 10(2), 887–902. https://doi.org/10.5194/cp-10-887-2014
- Landais, A., Barnola, J. M., Kawamura, K., Caillon, N., Delmotte, M., Van Ommen, T., et al. (2006). Firn-air delta N-15 in modern polar sites and glacial-interglacial ice: A model-data mismatch during glacial periods in Antarctica? *Quaternary Science Reviews*, 25(1–2), 49–62. https://doi.org/10.1016/j.quascirev.2005.06.007
- Lee, J. E., Brook, E. J., Bertler, N. A. N., Buizert, C., Baisden, T., Blunier, T., et al. (2020). An 83,000-year-old ice core from Roosevelt Island, Ross Sea, Antarctica. Climate of the Past, 16(5), 1691–1713. https://doi.org/10.5194/cp-16-1691-2020
- Markle, B. R., Steig, E. J., Roe, G. H., Winckler, G., & McConnell, J. R. (2018). Concomitant variability in high-latitude aerosols, water isotopes and the hydrologic cycle. *Nature Geoscience*, 11, 853–859. https://doi.org/10.1038/s41561-018-0210-9
- Masson-Delmotte, V., Hou, S., Ekaykin, A., Jouzel, J., Aristarain, A., Bernardo, R. T., et al. (2008). A review of Antarctic surface snow isotopic composition: Observations, atmospheric circulation, and isotopic modeling. *Journal of Climate*, 21(13), 3359–3387. https://doi.org/10.1175/2007jcli2139.1
- Masson-Delmotte, V., Stenni, B., Pol, K., Braconnot, P., Cattani, O., Falourd, S., et al. (2010). EPICA Dome C record of glacial and interglacial intensities. *Quaternary Science Reviews*, 29(1), 113–128. https://doi.org/10.1016/j.quascirev.2009.09.030
- Mayewski, P. A., Meeker, L. D., Twickler, M. S., Whitlow, S., Yang, Q., Lyons, W. B., & Prentice, M. (1997). Major features and forcing of high-latitude northern hemisphere atmospheric circulation using a 110,000-year-long glaciochemical series. *Journal of Geophysical Research*, 102(C12), 26345–26366. https://doi.org/10.1029/96jc03365
- Menking, J. A., Brook, E. J., Shackleton, S. A., Severinghaus, J. P., Dyonisius, M. N., Petrenko, V., et al. (2019). Spatial pattern of accumulation at Taylor Dome during Marine Isotope Stage 4: Stratigraphic constraints from Taylor Glacier. *Climate of the Past*, 15(4), 1537–1556. https://doi.org/10.5194/cp-15-1537-2019
- Monnin, E., Steig, E. J., Siegenthaler, U., Kawamura, K., Schwander, J., Stauffer, B., et al. (2004). Evidence for substantial accumulation rate variability in Antarctica during the Holocene, through synchronization of CO₂ in the Taylor Dome, Dome C and DML ice cores. *Earth and Planetary Science Letters*, 224(1–2), 45–54. https://doi.org/10.1016/j.epsl.2004.05.007
- Morse, D. L., Waddington, E. D., Marshall, H.-P., Neumann, T. A., Steig, E. J., Dibb, J. E., et al. (1999). Accumulation rate measurements at Taylor Dome, East Antarctica: Techniques and strategies for mass balance measurements in polar environments. *Geografiska Annaler Series A: Physical Geography*, 81(4), 683–694. https://doi.org/10.1111/j.0435-3676.1999.00096.x
- Otto-Bliesner, B. L., Brady, E. C., Zhao, A., Brierley, C. M., Axford, Y., Capron, E., et al. (2021). Large-scale features of Last Interglacial climate: Results from evaluating the lig127k simulations for the Coupled Model Intercomparison Project (CMIP6)-Paleoclimate Modeling Intercomparison Project (PMIP4). Climate of the Past, 17(1), 63–94. https://doi.org/10.5194/cp-17-63-2021
- Parrenin, F., Barker, S., Blunier, T., Chappellaz, J., Jouzel, J., Landais, A., et al. (2012). On the gas-ice depth difference (Δdepth) along the EPICA Dome C ice core. Climate of the Past, 8(4), 1239–1255. https://doi.org/10.5194/cp-8-1239-2012

BUIZERT 11 of 12



- Parrenin, F., Bazin, L., Capron, E., Landais, A., Lemieux-Dudon, B., & Masson-Delmotte, V. (2015). IceChrono1: A probabilistic model to compute a common and optimal chronology for several ice cores. *Geoscientific Model Development*, 8(5), 1473–1492. https://doi.org/10.5194/gmd-8-1473-2015
- Rhodes, R. H., Brook, E. J., Chiang, J. C. H., Blunier, T., Maselli, O. J., McConnell, J. R., et al. (2015). Enhanced tropical methane production in response to iceberg discharge in the North Atlantic. *Science*, 348(6238), 1016–1019. https://doi.org/10.1126/science.1262005
- Schmittner, A., Urban, N. M., Shakun, J. D., Mahowald, N. M., Clark, P. U., Bartlein, P. J., et al. (2011). Climate sensitivity estimated from temperature reconstructions of the last glacial maximum. *Science*, 334(6061), 1385–1388. https://doi.org/10.1126/science.1203513
- Schwander, J. (1989). The transformation of snow to ice and the occlusion of gases. In H. Oescher, & C. C. Langway (Eds.), The Environmental record in glaciers and ice sheets (pp. 53–67). John Wiley.
- Schwander, J., Sowers, T., Barnola, J. M., Blunier, T., Fuchs, A., & Malaize, B. (1997). Age scale of the air in the summit ice: Implication for glacial-interglacial temperature change. *Journal of Geophysical Research-Atmospheres*, 102(D16), 19483–19493. https://doi.org/10.1029/97jd01309
- Schwander, J., & Stauffer, B. (1984). Age difference between polar ice and the air trapped in its bubbles. *Nature*, 311(5981), 45–47. https://doi.org/10.1038/311045a0
- Seierstad, I., Abbott, P., Bigler, M., Blunier, T., Bourne, A., Brook, E. J., et al. (2014). Consistently dated records from the Greenland GRIP, GISP2 and NGRIP ice cores for the past 104 ka reveal regional millennial-scale isotope gradients with possible Heinrich Event imprint. *Quaternary Science Reviews*, 106, 29–46. https://doi.org/10.1016/j.quascirev.2014.10.032
- Seltzer, A. M., Ng, J., Aeschbach, W., Kipfer, R., Kulongoski, J. T., Severinghaus, J. P., & Stute, M. (2021). Widespread six degrees Celsius cooling on land during the Last Glacial Maximum. *Nature*, 593(7858), 228–232. https://doi.org/10.1038/s41586-021-03467-6
- Severinghaus, J. P., Sowers, T., Brook, E. J., Alley, R. B., & Bender, M. L. (1998). Timing of abrupt climate change at the end of the Younger Dryas interval from thermally fractionated gases in polar ice. *Nature*, 391(6663), 141–146. https://doi.org/10.1038/34346
- Simpson, M. J. R., Milne, G. A., Huybrechts, P., & Long, A. J. (2009). Calibrating a glaciological model of the Greenland ice sheet from the Last Glacial Maximum to present-day using field observations of relative sea level and ice extent. *Quaternary Science Reviews*, 28(17–18), 1631–1657. https://doi.org/10.1016/j.quascirev.2009.03.004
- Sowers, T., Bender, M., Raynaud, D., & Korotkevich, Y. S. (1992). δ¹⁵N of N₂ in air trapped in polar ice: A tracer of gas transport in the firn and a possible constraint on ice age-gas age differences. *Journal of Geophysical Research*, 97(D14), 15683–15697. https://doi.org/10.1029/92jd01297
- Svensson, A., Dahl-Jensen, D., Steffensen, J. P., Blunier, T., Rasmussen, S. O., Vinther, B. M., et al. (2020). Bipolar volcanic synchronization of abrupt climate change in Greenland and Antarctic ice cores during the last glacial period. *Climate of the Past*, 16(4), 1565–1580. https://doi.org/10.5194/cp-16-1565-2020
- Tierney, J. E., Zhu, J., King, J., Malevich, S. B., Hakim, G. J., & Poulsen, C. J. (2020). Glacial cooling and climate sensitivity revisited. *Nature*, 584(7822), 569–573. https://doi.org/10.1038/s41586-020-2617-x
- Veres, D., Bazin, L., Landais, A., Toyé Mahamadou Kele, H., Lemieux-Dudon, B., Parrenin, F., et al. (2013). The Antarctic ice core chronology (AICC2012): An optimized multi-parameter and multi-site dating approach for the last 120 thousand years. Climate of the Past, 9(4), 1733–1748. https://doi.org/10.5194/cp-9-1733-2013
- Werner, M., Jouzel, J., Masson-Delmotte, V., & Lohmann, G. (2018). Reconciling glacial Antarctic water stable isotopes with ice sheet topography and the isotopic paleothermometer. *Nature Communications*, 9(1), 3537. https://doi.org/10.1038/s41467-018-05430-y

BUIZERT 12 of 12